COMBINED THERMOELASTIC AND PHOTOELASTIC FULL-FIELD STRESS MEASUREMENT

Deonna Woolard, Mark Hinders, and Chris Welch
Department of Applied Science
College of William and Mary
Williamsburg, VA 23187

INTRODUCTION

Accurate determination of stress distributions is essential in assessing the structural integrity of a component. Photoelasticity and thermoelasticity are full field nondestructive methods used to measure the stress state of an object.

Photoelasticity has been used for decades to accurately measure surface strains in a structure. In this method the test part, complex or not, is first coated with a strain-sensitive plastic coating and then subjected to an external load. The strains which exist throughout the part and over its surface are transferred to the coating and observed as optical interference fringes with a reflection polariscope. Two different fringe patterns are produced with the polariscope -- isochromatics via circular polarization and isoclinics via linear polarization. Isochromatic fringes appear as a series of successive and contiguous different-colored bands each representing a different degree of birefringence corresponding to the underlying strain. The patterns can be read like a topographic map to visualize the stress distribution over the surface of the coated test part. The isoclinic fringes appear as black bands providing the direction of the principal strain [1-2]. Now that digital cameras and image processing are common, photoelasticity is undergoing a renaissance.

Whereas photoelasticity is an optical method, thermoelasticity is based on temperature changes induced by expansion and compression of the test part. Although this coupling between mechanical deformation and thermal energy has been known for over a century, it has only been recently that this phenomenon has been exploited as a means of experimental stress analysis. The heat generated from the thermoelastic effect is small -- 0.2°C for mild steel just below its yielding point -- requiring thermoelastic stress analysis to be performed under a dynamic loading condition of a sufficiently high frequency to maintain an effectively adiabatic state in the material [3]. For practical thermoelastic measurements using infrared thermography, the object under examination must have a highly emissive surface. For objects with low emissivity, such as metallic surfaces, a coating must be added, such as flat black paint.

COMBINATION OF THERMOELASTICITY AND PHOTOELASTICITY

Thermoelastic signals are proportional to the sum of the principal stresses

$$\Delta T = \left(\frac{-\alpha T}{\rho C_p}\right)(\sigma_1+\sigma_2) \tag{1}$$

(α is the thermal conductivity, ρ is the density, C_p is the specific heat capacity) whereas photoelasticity measures the difference of the principal stresses plus the principal stress

Review of Progress in Quantitative Nondestructive Evaluation, Vol. 18
Edited by Thompson and Chimenti, Kluwer Academic/Plenum Publishers, 1999

direction

$$\sigma_1-\sigma_2=\left(\frac{E}{1+\nu}\right)\left(\frac{N_n\lambda}{2kt}\right) \quad (2)$$

(E is the modulus of elasticity of the test material, ν is Poisson's ratio of the test material, N_n is the normal incident fringe order, λ is the wavelength of light, t is the thickness of the photoelastic coating, and k is the strain-optic coefficient of the coating). With each system it is difficult, sometimes impossible, to determine the individual stress components without the aid of a free surface. Several methods have been employed with photoelasticity to find a solution to this problem. One method involves the drilling of small circular holes over the surface of the testing object, the diameter of which is on the order of the thickness of the photoelastic coating, creating numerous traction free boundaries [4]. Another method combines normal incidence photoelastic measurements with oblique incidence measurements. The problem with this procedure is that the oblique incident measurements are much more difficult and time consuming compared to normal incidence. In addition, for certain strain states, significant errors can result from small inaccuracies in the measured fringe orders producing large errors in the calculated strains. Geometric details such as small fillets, reentrant corners, physical obstructions, etc., will often prevent the use of oblique incidence photoelastic measurements [5].

With the combination of the thermoelastic and photoelastic stress measurement systems, the full-field stress tensor can be determined with few geometric limitations. The key in linking the two system is the identification of a coating that is both highly emissive (thermoelastic) and birefringent (photoelastic). A partial-integration of thermoelasticity with photoelasticity was done in 1996 by S. Barone and E.A. Patterson. The two stress measurements were applied to the *opposite faces* of a plate with a central circular hole. They claim that the information could be obtained sequentially on the same face if the photoelastic coating could be bonded to the painted surface in the thermoelastic test or levered off with a scalpel before painting for thermoelastic analysis [6].

DUAL USE COATING: IDENTIFICATION AND CHARACTERIZATION

The photoelastic coating is made up of two layers -- a clear, isotropic plastic made from polycarbonate, polystyrene, or epoxy followed by a reflective layer comprised of metallic flakes suspended in an epoxy or an adhesive. Because of the nature of the coating requirements for photoelastic stress analysis, a birefringent coating must be made to work with the thermoelastic measurements for it requires only a high emissive surface. A solution to this mismatched coating requirement is to have the clear plastic be opaque to the infrared camera operating in the 3-5 μm region. Figure 1 shows the thermoelastic and photoelastic results for a plate with a centrally located hole in vertical tension.

The polycarbonate sheet used in this test measured 250 μm with a 500 μm adhesive reflective backing. Because of the thermally insulating properties of the polycarbonate, a thinner coating would facilitate a more defined thermoelastic image. For this reason a search was conducted on other photoelastic coatings and reflective backings. Figure 2 show the results of nine backings tested in the presence of polarized light. White light was passed through a polarizer, reflected off the samples, and passed through an analyzer set parallel (light field) and perpendicular (dark field) to that of the polarizer. All samples were compared to that of number seven, a commercially available photoelastic reflective adhesive used in the thermo/photoelastic data obtained in figure 1. It should be noted that sample nine was also a commercially available reflective backing that has been taken off the market due to the difficulty in its application process. Analysis of figure 2 shows samples one and two to be nearly identical to that of the industry standard. Sample one, a metallic spray paint, had a thickness measuring 10 μm whereas sample two, a gray high heat spray paint, had a thickness of 50 μm.

Testing was not limited to the reflective backings. Several birefringent polymer films were obtained that varied in color from clear to a brownish-orange, in optical transmission from transparent to opaque in the visible, and in thickness from 25 μm to 75 μm. Although

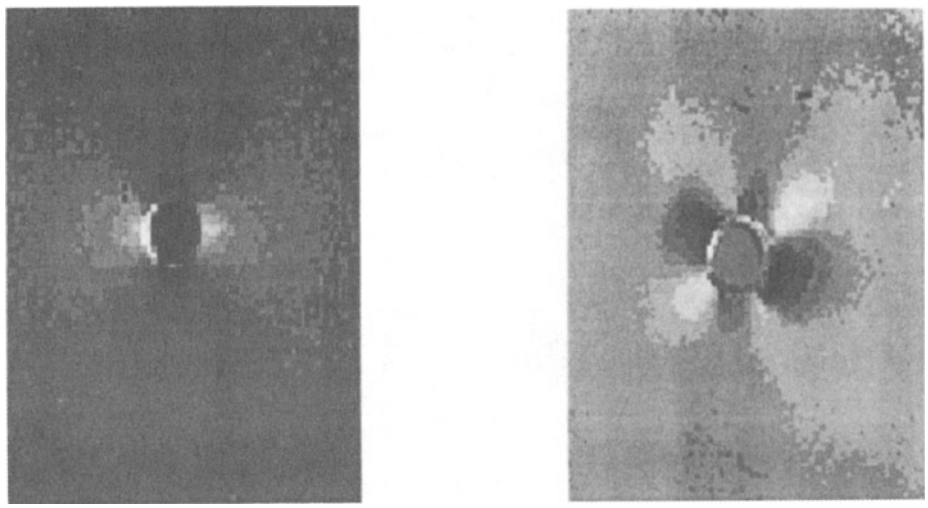

Figure 1. Typical thermoelastic (left) and photoelastic (right) responses from a polycarbonate sheet mounted to a plate with a central hole in vertical tension.

these materials should be opaque in the IR due to their chemical structure, testing of these films in the 3-5 μm IR showed otherwise. One possible reason is that the film thickness was too thin to show total opaqueness. Increasing the thickness or the addition of other chemicals may allow the film to become totally opaque in the 3-5 μm IR band. Other materials tested were polymethyl methacrylate (PMMA) and polyBisphenol-A carbonate. These materials started as solids before being dissolved in a solvent. It was found that similar solvents existed in the paints which caused the dried paint to rewet resulting in some mixing of the layers.

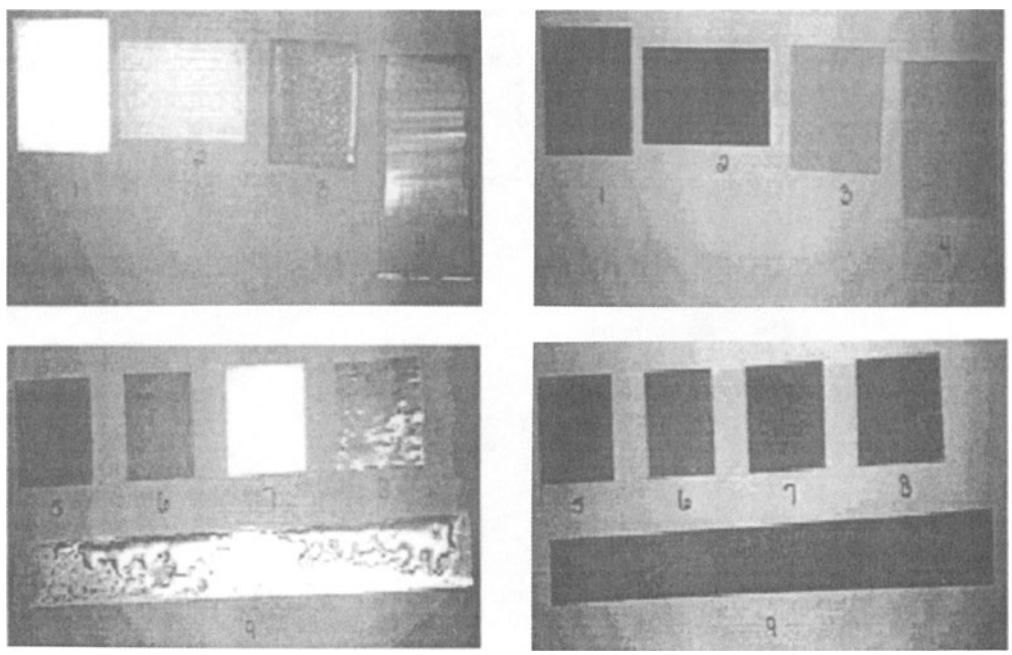

Figure 2. Comparative study of reflective backing candidates. The left images are taken using polarizers that are parallel (light field) and the right images using polarizers that are perpendicular (dark field).

ELECTRODYNAMIC MODELING OF THE PHOTOELASTIC COATING

A better understanding of the generation of fringes with applied load was needed for the combination of thermoelasticity with photoelasticity. Several theories exist for the explanation of photoelastic fringes [7-10], but no one theory alone was adequate for our purposes. Through a combination of these theories, a model has been developed for the simulation of photoelastic fringes given the stress distribution.

The origin of the photoelastic effect is associated with the change in the density of the medium resulting in the change in the index of refraction. An isotropic material becomes anisotropic when subjected to an applied stress or induced strain. A light wave propagating through an anisotropic material can be decomposed into two light waves (ordinary and extraordinary) each with different velocities and perpendicular polarizations. The relative retardation between these two waves is the difference in their optical path length

$$\delta = t\,(n_e - n_o) \tag{3}$$

where n is the index of refraction and t is the distance traveled in the medium. Brewster's Law connects the difference in the index of refraction with the difference in principal strains by

$$(n_1 - n_2) = K\,(\varepsilon_1 - \varepsilon_2) \tag{4}$$

where K is defined as the strain-optic coefficient and is a property of the material. A combination of equations (3) and (4) yields the general photoelastic equation

$$(\varepsilon_1 - \varepsilon_2) = \frac{\delta}{t\,K} = \frac{N\,\lambda}{t\,K} \tag{5}$$

seen in equation (2) without the factor of 1/2 because the light wave reflects off the back surface of the photoelastic coating doubling its path length.

The relationship between the electric field and the electric displacement is then written

$$E_i = \kappa_{ij}\,D_j \tag{6}$$

where κ_{ij} is the impermittivity tensor equal to the reciprocal of the permittivity. With the impermittivity tensor related to the principal index of refraction

$$\frac{1}{n^2} = \varepsilon_0\,\kappa, \tag{7}$$

an applied force causes a small change in the index of refraction which allows equation (7) to be expanded in terms of the total applied field

$$\kappa_{ik} = \kappa^0_{ik} + \left(\frac{1}{\varepsilon_0}\right) q_{ijkm} T_{jm} \quad \text{for stress and}$$
$$\kappa_{ik} = \kappa^0_{ik} + \left(\frac{1}{\varepsilon_0}\right) p_{ijkm} S_{jm} \quad \text{for strain.} \tag{8}$$

The tensor q_{ijkm} contains the stress-optic values whereas p_{ijkm} contains the strain-optic values which are related through the elastic stiffness constants by

$$p_{ijkl} = q_{ijmn} c_{mnkl}. \tag{9}$$

The electromagnetic model incorporates a z-propagating plane wave normally incident upon a birefringent coating of thickness d. The plane wave passes through a polarizer

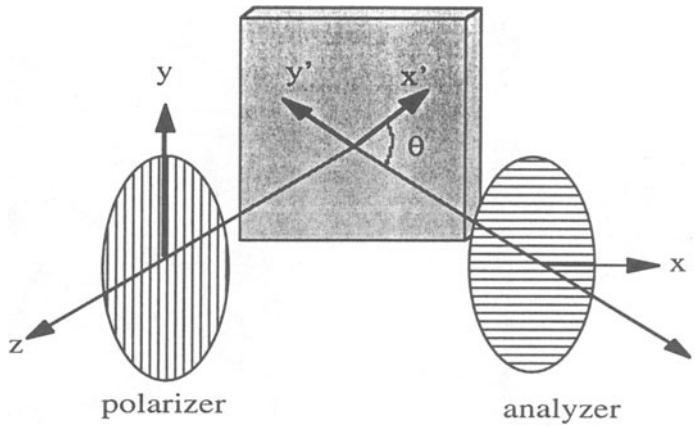

Figure 3. Coordinate systems for the electromagnetic model -- the primed system for the material and the unprimed for the measurement coordinates.

aligned along the *y*-axis, interacts with the stressed medium, reflects off the back surface of the photoelastic coating, and then passes through an analyzer aligned along the *x*-axis. Two coordinate systems are used in this model -- a primed system for the material coordinates and an unprimed system for the measurement system (figure 3). The electromagnetic waves inside and outside of the photoelastic material take the form

$$\begin{aligned}
\vec{E_{I'}} &= \hat{x}' A_x \cos(\vartheta-\phi) \exp[-ik_0 z] + \hat{y}' A_y \sin(\vartheta-\phi) \exp[-ik_0 z] \\
\vec{E_{R'}} &= \hat{x}' B_x \exp[ik_0 z] + \hat{y}' B_y \exp[ik_0 z] \\
\vec{E_{T'}} &= \hat{x}' \kappa_{x'x'} D_e \exp\left[-\frac{i\omega z}{\sqrt{\nu\kappa_{x'x'}}}\right] + \hat{y}' \kappa_{y'y'} D_o \exp\left[-\frac{i\omega z}{\sqrt{\nu\kappa_{y'y'}}}\right] \\
\vec{E_{TR'}} &= \hat{x}' \kappa_{x'x'} D_e' \exp\left[\frac{i\omega z}{\sqrt{\nu\kappa_{x'x'}}}\right] + \hat{y}' \kappa_{y'y'} D_o' \exp\left[\frac{i\omega z}{\sqrt{\nu\kappa_{y'y'}}}\right]
\end{aligned} \tag{10}$$

where ν is the reciprocal of the permeability, ϕ is the angle from the y-axis by which the polarizer and analyzer rotate about the z-axis maintaining their perpendicular alignment, and θ is the angle between the primed and unprimed systems which is determined by x'-axis aligning to the direction of the strain at a each point in the image. Using (10) with the appropriate electromagnetic boundary conditions allows the calculation of the coefficients B_x and B_y. The reflected wave is finally passed through the analyzer and converted into an intensity expression written as

$$I = (A_{ex} - A_{ox})^2 + (A_{ey} + A_{oy})^2 - 4(A_{ey}A_{oy} - A_{ex}A_{ox}) \sin^2\left(\frac{\delta}{2}\right) \tag{11}$$

where the A's are the amplitudes components of the reflected ordinary and extraordinary waves. The retardation, δ, is calcualted as

$$\delta = \text{Arctan}\left[\frac{-n_e \sin\left(\frac{2d\omega}{\sqrt{\nu\kappa_{xx}}}\right)}{\sin^2\left(\frac{d\omega}{\sqrt{\nu\kappa_{xx}}}\right) - n_e^2 \cos^2\left(\frac{d\omega}{\sqrt{\nu\kappa_{xx}}}\right)}\right] - \text{Arctan}\left[\frac{-n_o \sin\left(\frac{2d\omega}{\sqrt{\nu\kappa_{yy}}}\right)}{\sin^2\left(\frac{d\omega}{\sqrt{\nu\kappa_{yy}}}\right) - n_o^2 \cos^2\left(\frac{d\omega}{\sqrt{\nu\kappa_{yy}}}\right)}\right]. \tag{12}$$

Results obtained from equation (11) with $\phi = 0^\circ$ can be seen in figure 4 for a central hole in a plate under vertical tension.

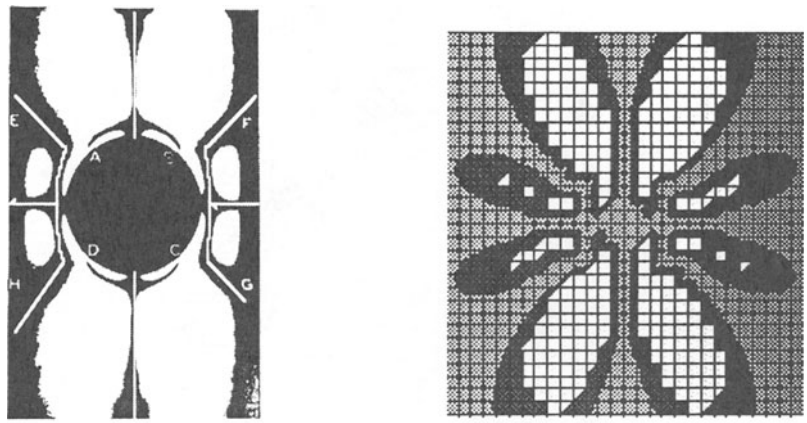

(a) (b)

Figure 4. Experimental [2] versus theoretical photoelastic intensity images with $\phi = 0°$. Figure (a) has the isoclinic lines drawn upon the image.

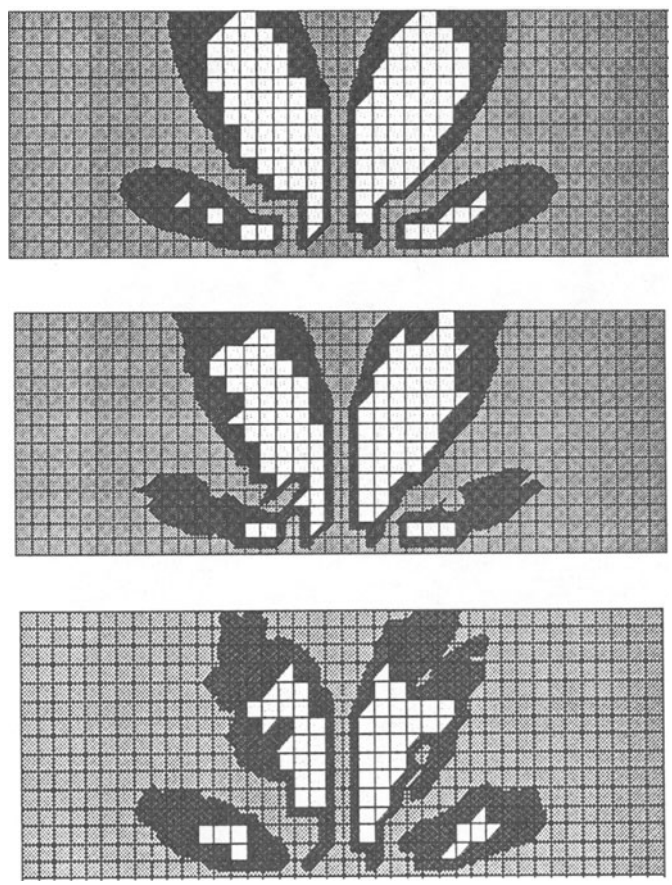

Figure 5. (top) Photoelastic image at $\phi = 0°$ for a perfect reflector at normal incidence, (middle) 25% depolarization at the reflecting layer, (bottom) 25% depolarization plus 5° off normal incidence.

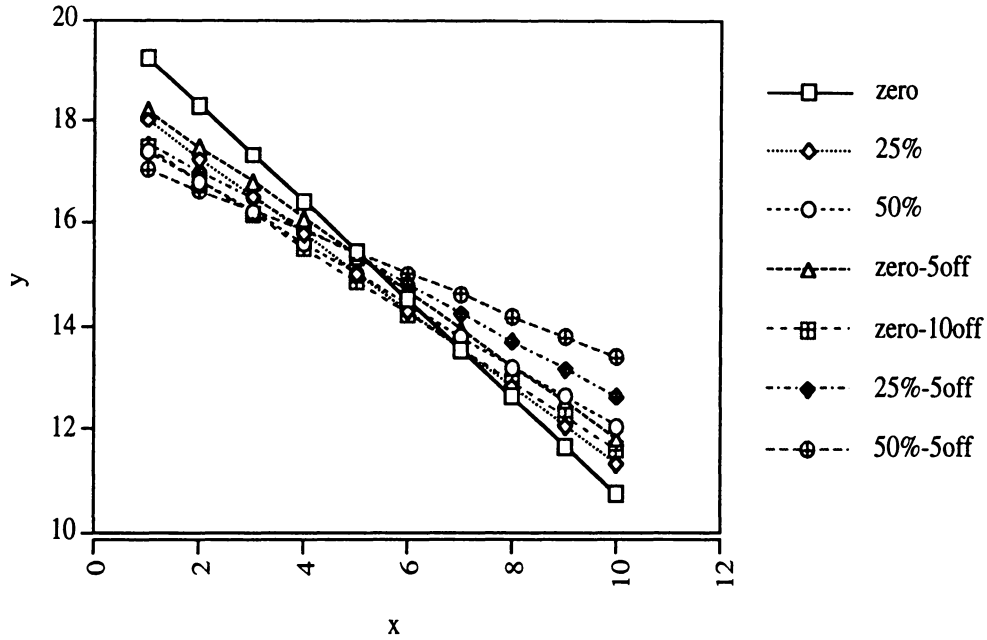

Figure 6. Best fit linear isoclinic line drawn between the left large and small lobes seen in figure 5.

Calculations to this point assumed a perfect reflecting backing at normal incidence. Incorporating an imperfect reflector which randomly transfers some of the energy from the ordinary to extraordinary wave plus the addition of less than normal incidence will allow us to study how the reflective backing affects the photoelastic signal. Figure 5 shows that as the reflective layer become less of a perfect reflector, the photoelastic image changes. More changes occur when a slightly less than normal incidence is introduced.

The physical significance of this changing image due to imperfect reflections and slightly less than normal incident light is in the drawing of the isoclinic lines. Noting that the isoclinic line between the large and small lobe is linear, a best fit line was determined for various depolarizations and angles off normal incidence. Figure 6 shows the best fit isoclinic line for various depolarizations and slightly off normal incidence. Figure 7 shows just how much the slope varies between the different cases.

CONCLUSION

With thermoelastic measurements providing the sum of the principal stresses and photoelasticity providing the difference of the principal stresses plus the principal direction, there is enough information to resolve the components of stress tensor over the full viewing area regardless of free surfaces. The two systems differ in surface preparation but have been linked through a polycarbonate coating which has been shown to work with both systems.

An electromagnetic wave theory has been developed which calculated the retardation between the extraordinary and ordinary waves . This was used to calculate photoelastic isoclinic lines which were found to vary as the reflective layer partially depolarized the wave at the back surface. The calculated slope of the isoclinic lines varied as much as 55% which would drastically affect the determination of the stress tensor components.

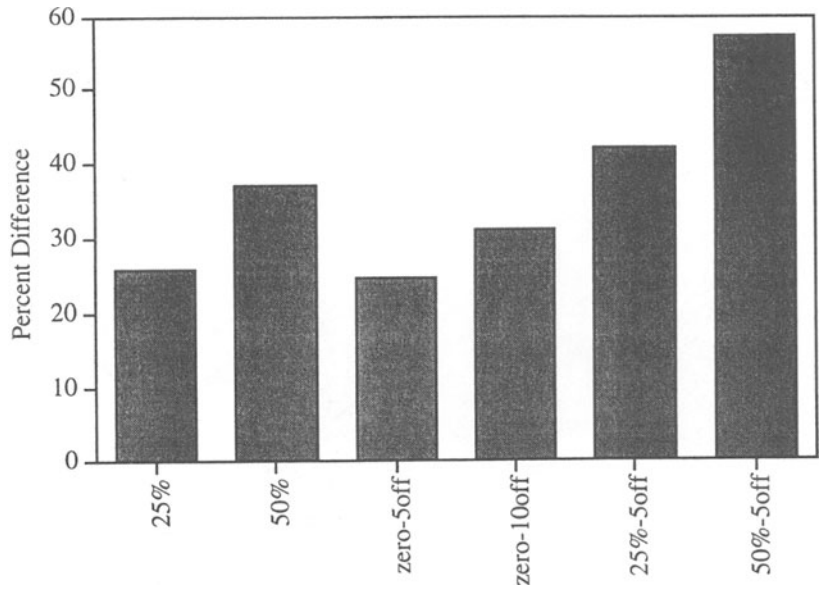

Figure 7. Percent difference in the slope of the best fit isoclinic line compared with the perfect reflecting, normal incidence case.

REFERENCES

1. "Introduction to Stress Analysis by the PhotoStress Method," Measurements Group Tech Note TN-702-1, Measurements Group, Inc., Raleigh, North Carolina.
2. *Photoelasticity, Volume 1,* Max Mark Frocht (John Wiley & Sons, Inc., New York, 1941).
3. *Thermoelastic Stress Analysis*, N. Harwood and W.M. Cummings, Eds. (Adam Hildger, Bristol, 1991).
4. A.J. Durelli and K. Rajaiah, "Determination of Strains in Photoelastic Coatings," *Experimental Mechanics,* Vol. 20, pp. 57-64 (1980).
5. "Separation of Principal Strains," Operating Instructions and Technical Manual for the 030-Series Reflection Polariscope, Measurements Group, Inc., Raleigh, North Carolina.
6. S. Barone and E.A. Patterson, "Full-field Separation of Principal Stresses by Combined Thermo-and Photoelasticity," *Experimental Mechanics,* Vol 36, pp. 318-324 (1996).
7. *Modern Optics,* Robert Guenther, Chapter 14 (John Wiley & Sons, New York, 1990).
8. *Electromagnetic Wave Theory, Second Edition,* Jin Au Kong, Chapter 2 (John Wiley & Sons, New York, 1990).
9. *Electrodynamics of Continuous Media, Volume 8,* L.D. Landau and E.M. Lifshitz (Permgamon Press, Oxford, 1960).
10. J.A. Brandao Farla, "A Perturbation Approach to the Analysis of Index Ellipsoid Deformations in Biaxial and Uniaxial Media," *Microwave & Optical Technology Letter,* Vol. 6, No. 11, pp. 657-660 (1993).